Luminescent Downshifting by Photo-Induced Sol-Gel Hybrid Coatings: Accessing Multifunctionality on Flexible Organic Photovoltaics via Ambient Temperature Material Processing

Diego Pintossi, Giovanni Iannaccone, Alessia Colombo, Federico Bella, Marja Välimäki, Kaisa-Leena Väisänen, Jukka Hast, Marinella Levi, Claudio Gerbaldi, Claudia Dragonetti, Stefano Turri, and Gianmarco Griffini*

A novel high-durability multifunctional organic–inorganic hybrid coating material is presented in this work as luminescent down-shifting (LDS) host matrix system for flexible organic photovoltaic (OPV) devices. Such new LDS coating is obtained by incorporating a convenient fluorescent organic dye in an appropriately functionalized fluoropolymeric resin that can be readily crosslinked by means of a dual-cure mechanism with a single-step ambient-temperature photo-induced sol–gel process. Due to its peculiar characteristics, the newly proposed system may be readily implemented in heat-sensitive flexible devices. By carefully tuning the amount of organic fluorophore in the hybrid coating material, a maximum increase in power conversion efficiency exceeding 4% is achieved on devices incorporating the new LDS layer with respect to control systems. This represents the highest efficiency enhance-ment reported to date on flexible OPVs by means of a polymer-based LDS layer. In addition, long-term accelerated weathering tests (>550 h) highlight the excellent stability of LDS-coated OPV devices, which can retain 80% of their initial performance, as opposed to the dramatic efficiency decay experienced by control uncoated devices. The approach presented here opens the way to the straightforward incorporation of versatile multifunctional light-managing layers on flexible OPV systems for improved device efficiency and lifetime.

1. Introduction

Organic photovoltaics (OPV) based on conjugated polymers and fullerenes have been extensively investigated in recent years because of their potential for low-cost, light-weight, and flexible devices entirely fabricated by scal-able solution processing.[1]

Continuous research for new active materials and device architectures in this class of solar cells has recently led to power conversion efficiencies (PCEs) routinely exceeding the 10% landmark.[2] Despite several potential advantages of OPVs over conventional systems, there are still important pending issues to be overcome that partially prevent widespread adop-tion of this technology on a large scale. In particular, PCE and long-term opera-tional stability of OPV devices are still to be greatly improved before this technology can reliably enter the PV market arena.

In this context, relatively limited PCEs observed on OPV systems can be typically ascribed to the poor spectral matching between the absorption band of photo-active materials and the emission char-acteristics of the solar spectrum.[3] In order to enhance device PCEs, several strategies have been adopted in the past decades aimed at improving the spectral response of the OPV stack, including the use of highly performing low bandgap donor polymers[4] and the engineering of new device systems such as tandem or multi-junction architectures.[2,3,5] Although effective, all these approaches directly impact on the structure of the OPV system

D. Pintossi, Dr. G. Iannaccone, Prof. M. Levi, Prof. S. Turri, Dr. G. Griffini
Department of Chemistry
Materials and Chemical Engineering "Giulio Natta"
Politecnico di Milano
Piazza Leonardo da Vinci 32, 20133 Milano, Italy
E-mail: gianmarco.griffini@polimi.it

Dr. A. Colombo, Prof. C. Dragonetti
Department of Chemistry
Università degli Studi di Milano
Via Golgi 19, 20133 Milano, Italy

Dr. F. Bella, Prof. C. Gerbaldi
GAMELab
CHENERGY Group
Department of Applied Science
and Technology – DISAT
Politecnico di Torino
Corso Duca degli Abruzzi 24, 10129 Torino, Italy

M. Välimäki, K.-L. Väisänen, Prof. J. Hast
VTT Technical Research Centre of Finland
P.O. Box 1100, FI-90570 Oulu, Finland

(e.g., chemistry of the photoactive layer, energy levels within the device, interfacial engineering) and require the systematic implementation of extensive optimization protocols that can be typically applied only to a specific device configuration, without the possibility to be extended to other systems. As a result, accessing more general, system-independent strategies for improved OPV device performance is still a great challenge.

Besides efficiency, device lifetime represents another major target for successful OPV development.[6,7] In this context, the limited outdoor stability of OPV systems is typically the result of a multitude of combined external stresses that include high temperature, oxygen, moisture, and high-energy UV-light. Their synergistic negative action on device components mainly leads to irreversible changes in the bulk heterojunction (BHJ) morphology as well as in the photo-oxidation of photoactive materials, thus causing a dramatic drop in performance upon prolonged operation.[6–8] To address some of these issues, specific modifications to the chemistry of the photoactive layer have been proposed, including the use of (photo- or thermo-) crosslinkable photoactive layers[9] or the incorporation of thermo-cleavable side chains in the donor polymer.[10] While stable BHJ morphologies could be reproducibly obtained by means of these approaches, inferior device performance has been typically observed compared to traditional photoactive materials.[6] Another strategy consists in the application of external barrier layers incorporating optical (UV) filters to prevent OPV device exposure to harmful high-energy radiations and atmospheric agents (viz., oxygen and moisture), thus partially limiting photochemical degradation of the photoactive layer.[11]

More recently, luminescent downshifting (LDS) has been proposed as a viable holistic approach to simultaneously achieve enhanced efficiency and improved durability of PV devices. Upon the absorption of incident UV-photons by means of a luminophore embedded in a transparent matrix and their re-emission at longer wavelengths, device PCE can be enhanced due to the higher number of photons with appropriate frequencies reaching the photoactive materials. In addition, device stability can be improved as the UV portion of the incident light is filtered by the LDS luminophore and photodegradation of the photoactive material can be prevented.[12] Hovel et al. first reported the application of LDS layers to improve the performance of PV devices in 1979.[13] This approach has been extensively investigated in the following decades with encouraging results on several PV technologies, including silicon-based GaAs, CdTe, copper indium selenide, and dye sensitized solar cells.[14–17] As far as OPVs are concerned, LDS has found limited application, with most examples focusing on rigid devices. Despite providing encouraging results, the studies performed on rigid substrates offer limited scalability.[18–20] Therefore, the most interesting examples of LDS in the OPV field are those involving the use of flexible OPV devices fabricated by readily scalable solution processing and coated with roll-to-roll compatible LDS systems. In this context, an interesting demonstration has been very recently presented, involving the use of polymeric LDS coatings onto large OPV modules with promising results.[21] LDS layers for OPV applications typically rely on the use of conventional polymeric matrices (most typically, poly(methyl methacrylate)) that are known to suffer from limited outdoor stability,[22] the latter being a clear drawback for the design of LDS systems with long-term operational stability. Few examples of alternative LDS host matrices have been presented recently in the OPV literature,[18–20] but they demonstrated limited scalability to industrial level due to their relatively complex fabrication procedures that often require multi-step processing[19] or additional thermal treatments that may negatively affect the morphology of the underlying BHJ material.[19,20]

Within this framework, we report here the development of a novel high-durability multifunctional organic–inorganic hybrid coating material and its straightforward application as LDS host matrix system for flexible OPV devices. Such new LDS coating was obtained by incorporating a convenient pyridine-based fluorescent organic dye in an appropriately functionalized fluoropolymeric resin that can be readily crosslinked in one-pot at ambient conditions by means of a new dual-cure photo-induced sol–gel process. As such, this system is particularly suited for application on heat-sensitive flexible OPV devices, as the absence of additional thermal treatments to obtain the crosslinked coating eliminates the possibility of distortions in the substrate or degradation of the BHJ morphology. Judicious control over the amount of organic fluorophore in the coating material allowed to achieve a maximum increase in PCE exceeding 4% on devices incorporating the new LDS layer with respect to control systems. To the best of our knowledge, this represents the highest efficiency enhancement reported to date on flexible OPVs by means of a polymer-based LDS layer. These results were correlated with the photophysical properties of the LDS coating. In addition, long-term accelerated weathering tests (>550 h) highlighted the excellent stability of LDS-coated OPV devices, which proved to effectively retain 80% of their initial performance, as opposed to the dramatic efficiency drop experienced by uncoated control devices.

2. Results and Discussion

The hybrid multifunctional coating was obtained via a new photo-induced sol–gel process involving the UV-assisted room temperature reaction of an inorganic precursor (tetraethylorthosilicate, TEOS) with an appropriately functionalized copolymer based on chlorotrifluoroethylene-vinyl ether (CTFE-VE). Functionalization of the CTFE-VE resin was carried out by reacting all available hydroxyl groups in CTFE-VE with equimolar amounts of isocyanatoethyl methacrylate (IEM) and triethoxysilyl propyl isocyanate (IPTES) through the formation of urethane bonds (a detailed description of the synthetic procedure is presented in the Experimental Section). As a result, methacrylate and silane moieties could be incorporated into the same CTFE-VE backbone as pendant side groups, thus leading to the final functionalized methacrylate/silane resin (MS-resin, **Scheme 1**). In conventional alkoxysilane-based sol–gel processes, a sequence of interconnected reactions is ultimately responsible for the hydrolysis of the Si precursor (in most cases TEOS) and its subsequent condensation to form the final —O—Si—O— 3D network.[23] In these cases, the condensation step is normally promoted by prolonged medium-to-high temperature treatments (>150–200 °C) at ambient pressure, so as to induce

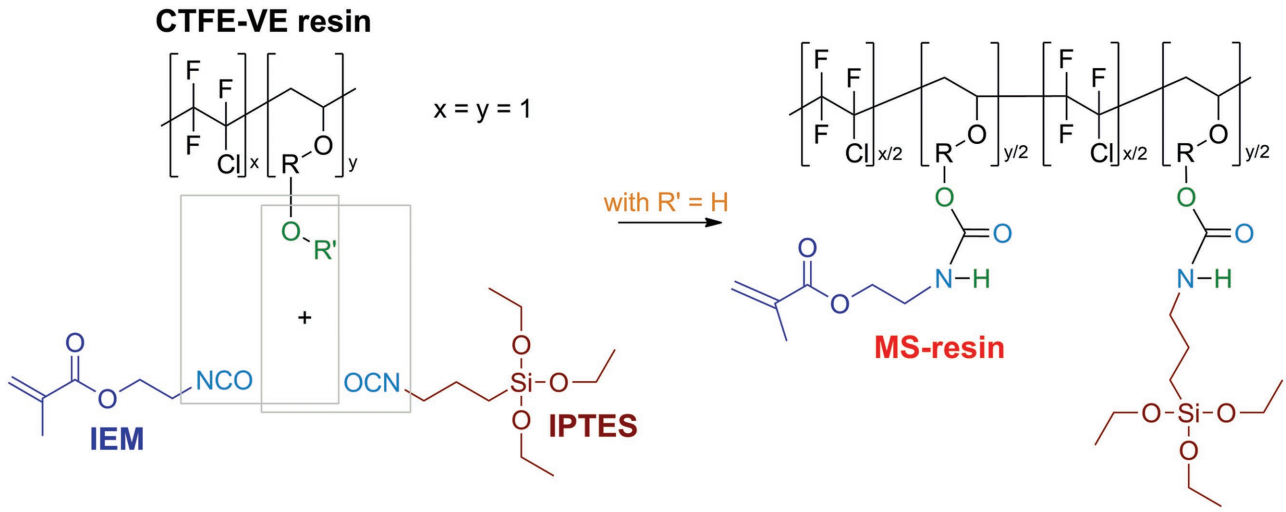

Scheme 1. Schematic illustration of the functionalization reaction between the CTFE-VE resin, IEM, and IPTES, leading to MS-resin.

evaporation of volatile byproducts and result in the formation of the final solid film.[24] Clearly, such thermal annealing steps are not compatible with the use of heat-sensitive plastic substrates such as poly(ethylene terephthalate) (PET), which exhibit maximum working temperatures in the 100–150 °C range. Therefore, application of this class of sol–gel materials to flexible devices is still a great challenge. In order to circumvent this problem, a novel strategy was proposed here based on the exploitation of the reactivity to UV-light of the methacrylate groups synthetically introduced in the functionalized MS-resin. Upon UV-irradiation in the presence of a radical photoinitiator, such methacrylate C=C double bonds undergo homolytic scission, thus triggering the radical photocrosslinking reaction of the MS-resin via radical polymerization. Concurrently, the exothermic process occurring during the UV-induced C=C bond cleavage can locally activate the −O−Si−O− polycondensation reactions between the −SiOH moieties originated from the hydrolysis of the –Si(OC_2H_5) groups in MS-resin and TEOS, ultimately leading to the concomitant formation of the inorganic SiO_2 network (**Scheme 2**) at ambient temperature. In this way, a fully crosslinked organic/inorganic hybrid coating (from here on referred to as H-coating) can be readily obtained in one-pot through a novel synthetic approach that eliminates the need of thermal post-treatments, thus opening the way for the use of such sol–gel systems onto heat-sensitive flexible substrates. In addition, the fluorinated nature of this new material combined with the highly interconnected organic/inorganic 3D network formed upon crosslinking is expected to provide prolonged outdoor durability to the coating.

In order to verify the occurrence of the crosslinking reaction, Fourier-transform infrared (FTIR) spectra were collected before and after UV irradiation of the sol (Figure S1, Supporting Information). The reduced intensity of the C=C double bond signal (1640 cm^{-1}) provides an evidence of the UV-induced double bond opening in the methacrylate groups, while the reduced intensity of the peaks associated to Si−OH (3700–3200 cm^{-1}) and Si−O−C (1110–1050 cm^{-1}) coupled with the increased intensity of the Si−O−Si signal (1090–1030 cm^{-1}) clearly demonstrate the effective occurrence of the polycondensation reaction of the inorganic component. Furthermore, to investigate the extent of crosslinking of the newly proposed coating system, the sol–gel precursor formulation was exposed to UV-light at ambient temperature and the chemical resistance of the so-formed H-coating was assessed by means of the solvent rubbing test (methyl ethyl ketone, MEK).[25] As a result of the highly crosslinked nature of the prepared material, the solid film was found to withstand over 100 continuous solvent double rubs, clearly indicating the successful formation of an interconnected organic/inorganic hybrid network immediately after UV-irradiation. An analogous behavior was observed on H-coatings formed upon exposure to UV-light at 0 °C (in an ice bath). This result rules out any possible thermal effect attributable to additional external heat sources and further confirms that the (methacrylate) C=C bond cleavage taking place during UV-irradiation can provide sufficient thermal energy to promote –SiOH polycondensation reactions and yield the fully crosslinked hybrid solid film (Scheme S1, Supporting Information). The successful formation of the interconnected hybrid organic/inorganic network was further confirmed after performing solvent rubbing tests on similar coating systems based on the same CTFE-VE resin functionalized only with IEM (OH:NCO = 1:1), which did not prove to withstand 100 solvent double rubs. Therefore, the superior solvent resistance of the H-coating compared to similar fully organic films can be reliably attributed to the successful polycondensation reaction of the inorganic component which leads to the formation of a fully crosslinked organic/inorganic hybrid network. Further evidence of the highly crosslinked nature of the UV-cured H-coating was obtained by immersing it into chloroform for 24 h. In accordance with the previous observations, no significant weight loss was registered on the material (residual gel content over 99%), again demonstrating efficient curing and excellent chemical resistance.

Differential scanning calorimetry (DSC) analyses were carried out on the H-coating to evaluate its thermal transitions. As shown in **Figure 1**a, the UV-cured material exhibits a single glass transition temperature (T_g), clearly indicating the monophasic nature of the system that results from the excellent

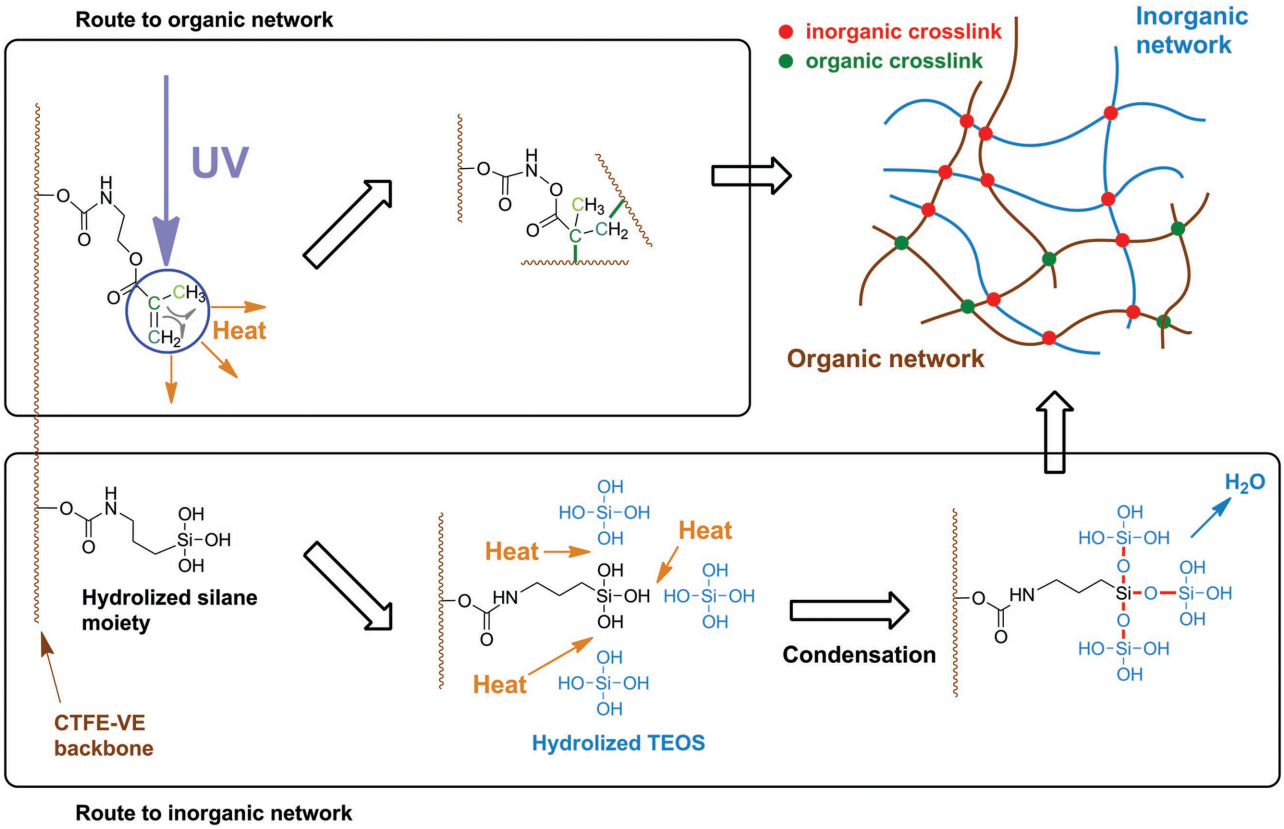

Scheme 2. Schematic illustration of the crosslinking reactions taking place in the coating upon UV irradiation under inert atmosphere. The opening of the double bond in the methacylate moieties (polyaddition) provides the heat necessary for the polycondensation reaction of the silanol groups, leading to a three-dimensional hybrid organic/inorganic network.

mutual compatibility of its organic (polymeric) and inorganic (Si-based) components. In particular, the T_g (180 °C, third scan measurement) was found to lie well above the maximum service temperatures commonly expected for PV devices (50–70 °C in the worst case scenarios),[26] thus confirming the suitability of this material for outdoor use in LDS applications. It is worth mentioning that, despite its high T_g, the H-coating was found to exhibit remarkable flexibility and high resistance to bending when applied in the form of very thin films (1 µm, as measured by optical profiler) onto flexible substrates. Indeed, images of the UV-cured samples deposited on PET substrates taken before and after several bending cycles (100 cycles, with radius of curvature equal to 1 cm) showed no visible cracks developed in the coating (Supporting Information, Figure S2) upon repeated

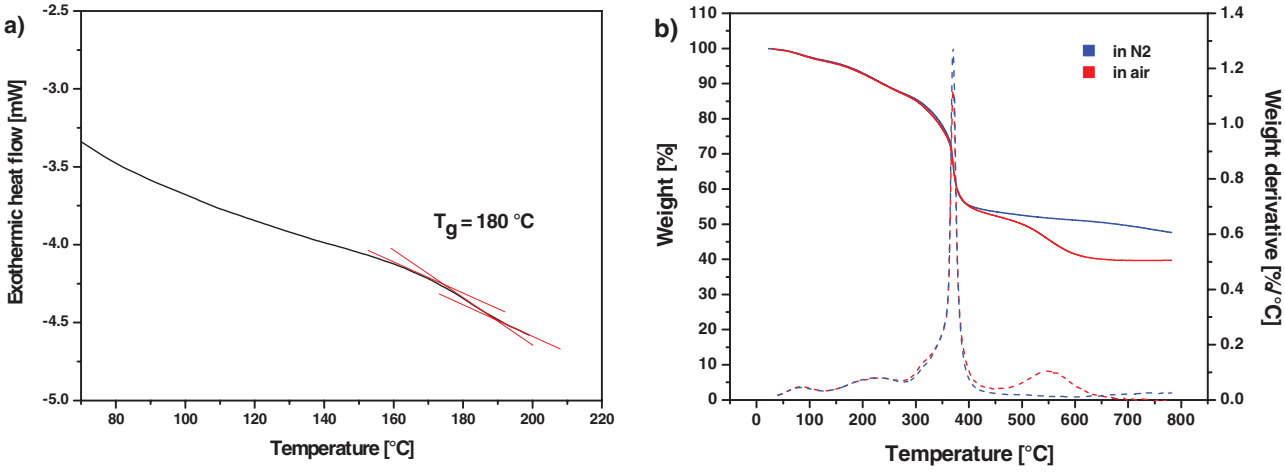

Figure 1. a) DSC trace for MS-resin. b) TGA curves (solid lines) and differential TGA traces (dashed lines) for MS-resin in air and nitrogen.

mechanical stresses. This behavior is of particular interest for optical applications (such as in the case of LDS), as the presence of non-negligible surface roughness on the coating can lead to undesirable light scattering that may ultimately result in detrimental photon losses. Conversely, thicker layers of H-coating were shown to be highly fragile, develop macroscopic cracks, and delaminate after few bending cycles.

To assess the thermal stability of the H-coating, thermogravimetric analysis (TGA) was performed both in air and under nitrogen flux. As shown in Figure 1b, the main weight loss event occurs at about 370 °C and it can be associated to the thermal degradation of the polymer (ether and ester linkage decomposition together with chain scission reactions).[17] Additional minor mass losses occurring at lower temperatures (<300 °C) are likely to be the result of the evaporation of solvents and byproducts of the hydrolysis and condensation reactions taking place during the formation of the solid film, or to the degradation of urethane linkages (150–250 °C). In particular, the boiling points of ethanol (EtOH, the solvent used in the sol–gel precursor formulation) and TEOS (the inorganic precursor) are 78 and 170 °C, respectively, which are compatible with the low-temperature mass losses observed in Figure 1b. In the case of TGA carried out in air, an additional final mass loss is observed at about 550 °C, likely ascribable to the complete decrosslinking and degradation of the organic (polymeric) component of the H-coating. Finally, it is worth noticing that even for very high temperatures (>700 °C) the hybrid material does not fully lose its mass, as the inorganic component in the H-coatings (SiO_2) is highly stable within the temperature range considered here. In particular, the amount of residual weight retained at 800 °C well correlates with the estimated theoretical content of SiO_2 in the solid film (Table S1, Supporting Information), taking into account that a small fraction of the initial weight is lost due to unreacted materials and trapped solvents evaporating at low temperatures (<200 °C).

An investigation of the wettability behavior of the new LDS coating was carried out by means of static contact angle measurements, using water and diiodomethane as probe liquids. The surface energy, with its polar and dispersive components (γ^p and γ^d, respectively), was calculated using the Owens, Wendt, Rabel, and Kaelble method.[27] Optical contact angle and surface energy values for bare PET and for H-coating are listed in **Table 1**. The moderately hydrophobic behavior of the coating is evident from the measured static water contact angle (93.5° ± 0.8°) (Figure S3, Supporting Information) and surface tension (30.57 mN m^{-1}). As a result, the presence of the H-coating on the PET substrate is expected to provide easier cleaning functionality to the underlying layers (the OPV device), thus preventing accumulation of dirt, dust, or solid particles during operational service. In addition, water ingress is expected to be significantly limited thanks to the fluorinated nature of the polymeric component in the coating, thus leading to prospective enhancement of device lifetime.

Table 1. Water and diiodomethane contact angles, together with total surface energy with its dispersive and polar components for MS-resin and bare PET substrate.

Coating	θ_{H2O} [°]	θ_{CH2I2} [°]	γ [mN m^{-1}]	γ^d [mN m^{-1}]	γ^p [mN m^{-1}]
Uncoated PET	63.2 ± 1.3	27.1 ± 1.0	51.23	39.22	12.01
H-coating	93.5 ± 0.8	57.2 ± 0.7	30.57	28.35	2.22

Following the preliminary analysis of the proposed hybrid sol–gel coating that highlighted its potential suitability as host matrix material for LDS applications, an adequate chromophore was needed to provide the new system with an additional optical functionality so as to obtain a truly multifunctional light-managing coating. In order to carry out LDS experiments on OPVs, devices based on the poly(3-hexylthiophene):[6,6]-phenyl-C_{61}-butyric acid methyl ester (P3HT:PCBM) BHJ were chosen as a reliable and extensively investigated platform. Indeed, such a photoactive blend is arguably the most widely studied material combination in the OPV field.[28] Therefore, straightforward approaches to improve the performance of P3HT:PCBM-based devices are likely to be of broad interest in the OPV community and can contribute significantly to the advancement of this technology. For LDS applications, the absorption and emission response of the selected luminophore must match that of the OPV photoactive material. In this work, the newly synthesized organic dye *trans*-5-(*p*-(*N*,*N*-diphenylamino)styril)-1,3-di(2-pyridyl)-benzene (**Figure 2**b, from here on referred to as PB-dye) was chosen as promising fluorescent doping species in the hybrid H-coating due to its favorable optical properties and relatively easy synthetic procedure. PB dye was synthetized following a slightly modified procedure with respect to recent literature.[29]

A preliminary functional characterization was carried out on PB-dye, based on five figures of merit (FoM) that take into account the optical properties of the luminophore: photoluminescence quantum yield (PLQY), absorption spectral matching, emission spectral matching, radiative overlap, and parasitic absorption (a detailed description of the different FoM is provided in the Supporting Information, with corresponding calculations for the PB-dye, Table S2, Supporting information).[15,30] The calculated FoM values are very similar to those reported for other photoluminescent systems successfully employed in LDS applications on different PV technologies.[16,17] Therefore, the selected PB-dye is expected to yield beneficial effects as fluorescent species for LDS applications in OPV devices.

The optical properties of the PB-dye were investigated by means of UV–vis and fluorescence spectroscopies. As shown in Figure 2a, a broad absorption band is observed centered at 375 nm, with an emission peak centered at 446 nm. As such, this dye is particularly suited for LDS applications on P3HT:PCBM-based OPV devices because the spectral response of the solar cell is low in the region where the dye absorbs photons, while it is relatively high in the portion of the spectrum where PB re-emits fluorescence photons. Based on these preliminary considerations, the PB-doped organic/inorganic hybrid LDS layer is expected to operate an efficient downshifting process when incorporated as top layer in P3HT:PCBM-based OPV devices.

In order to evaluate the functional response of the proposed LDS system constituted by the new hybrid H-coating matrix material embedding the fluorescent PB-dye, a systematic study was performed on OPV devices incorporating the LDS system as top coating layer. To this end, flexible inverted OPV devices with the architecture PET-indium tin oxide (ITO)/ZnO/P3HT:PCBM/PEDOT:PSS/silver (Figure 2b) were fabricated

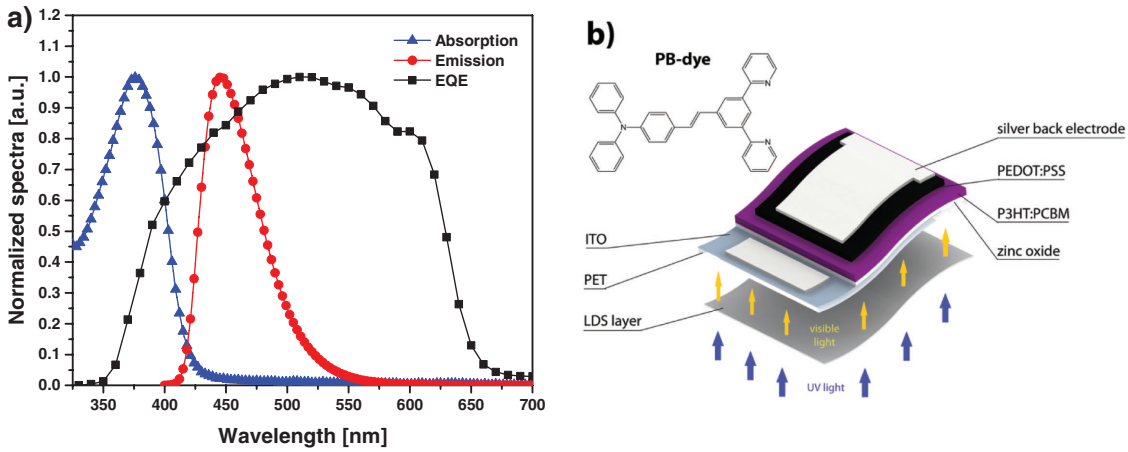

Figure 2. a) Absorption and emission spectra of the organic dye, superimposed to the external quantum efficiency (EQE) curve of the OPV device. b) schematic illustration of the LDS process and the molecular structure of the PB-dye incorporated in the LDS layer.

and encapsulated by cold lamination between two transparent PET foils. Subsequently, LDS coatings with increasing concentration of PB-dye were deposited onto the top side of the OPV devices, and the performance increase of the complete LDS system compared to the bare uncoated OPVs was measured under AM1.5G irradiation. **Table 2** and Figure S4 (Supporting Information) illustrate the variations in the PV parameters observed on OPV devices after application of the LDS layer at different PB concentrations. A clear performance enhancement is observed by gradually increasing PB concentration. In particular, the short circuit current density (J_{sc}) is found to undergo a nearly 5% increase when PB concentration in the LDS coating is raised up to 1 wt%, as it can be observed in **Figure 3**. This behavior may be correlated with the increasingly larger number of available photons with suitable wavelengths reaching the underlying solar cells as a consequence of the downshifting process. Consistently, no significant variations are observed in the same PB concentration range on the open-circuit voltage (V_{oc}) and fill factor (*FF*), further confirming that the LDS process mainly acts on the concentration of the charge carriers without affecting the morphology of the BHJ or the electrical (shunt and series) resistances in the device. By further increasing the concentration of the luminescent species (>1 wt%), the performance of the LDS-OPV systems is found to worsen significantly. As previously reported on analogous systems,[31] such performance decrease observed at high luminophore concentrations may be correlated with the partial overlap between absorption and emission spectra of the PB fluorescent dye. In particular, a higher fluorophore concentration (higher optical density) entails a higher probability for emitted photons to be reabsorbed by adjacent dye molecules, thus reducing the probability of successful transmission of fluorescence photons to the underlying BHJ, consequently leading to a lower concentration of charge carriers in the photoactive layer. In the system presented here, such an effect starts to be relevant for dye concentrations exceeding 1 wt%.[31] In addition, by further increasing the concentration of fluorescent molecule in the LDS layer, a progressively lower solubility of PB-dye in the H-coating was observed, which was found to be relatively poor for concentrations higher than 2 wt%. This effect may lead to the formation of nonfluorescent dimers and aggregates that inevitably reduce the PLQY of the LDS layer and, in turn, lower the OPV performance.[16,32] It is worth noticing that a slight performance improvement with respect to the uncoated OPV device was observed also in the presence of the bare H-coating (0 wt% PB). This behavior may be explained by considering the lower refractive index of the fluorinated H-coating (1.46 for the CTFE-VE resin precursor)[33] compared to that of PET (1.58–1.64) that induces some antireflective properties to the coated system even in the absence of any luminophore in the coating, thus allowing for a modest increase in J_{sc}.

In the attempt to further confirm the downshifting effect observed on LDS-coated OPV devices at increasing PB-dye concentration, an additional investigation was performed by

Table 2. Device parameters for the reference and LDS-coated devices.

	V_{oc} [V]	J_{sc} [mA cm^{-2}]	*FF* [a.u.]	PCE [%]	J_{sc} improvement [%]	PCE improvement [%]
Reference	0.565 ± 0.010	6.518 ± 0.030	0.552 ± 0.013	2.033 ± 0.010	–	–
0 wt% PB	0.564 ± 0.011	6.643 ± 0.027	0.556 ± 0.011	2.076 ± 0.012	+1.921 ± 0.361	+2.118 ± 0.095
0.1 wt% PB	0.566 ± 0.010	6.660 ± 0.028	0.556 ± 0.013	2.079 ± 0.009	+2.176 ± 0.096	+2.261 ± 0.135
0.5 wt% PB	0.566 ± 0.012	6.724 ± 0.030	0.556 ± 0.012	2.094 ± 0.010	+3.172 ± 0.292	+2.983 ± 0.097
1 wt% PB	0.564 ± 0.010	6.843 ± 0.027	0.556 ± 0.010	2.114 ± 0.009	+4.990 ± 0.813	+3.982 ± 0.885
2 wt% PB	0.566 ± 0.011	6.634 ± 0.031	0.555 ± 0.013	2.069 ± 0.012	+1.791 ± 0.496	+1.773 ± 0.891
5 wt% PB	0.564 ± 0.010	6.571 ± 0.027	0.553 ± 0.012	2.055 ± 0.010	+0.822 ± 0.038	+1.090 ± 0.461

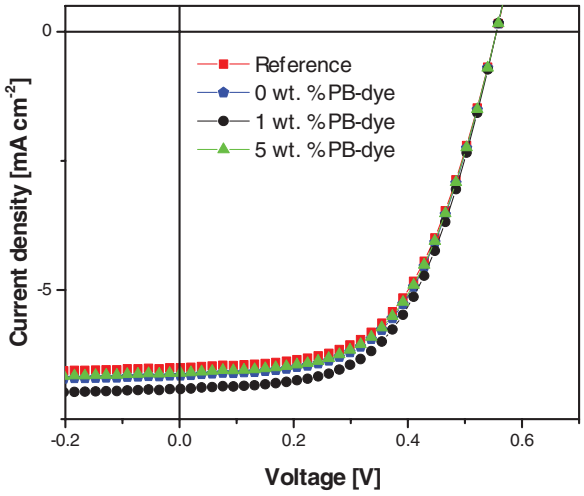

Figure 3. *JV* curves of the reference and coated OPV devices.

measuring the external quantum efficiency (EQE) of devices coated with LDS layers incorporating increasing concentrations of PB-dye. **Figure 4** clearly shows an increase in EQE at low PB-dye concentrations in the region of the spectrum below 400 nm, where the absorption peak of the luminophore is found. This observation confirms the beneficial action of the organic dye in the LDS system, which is able to absorb short-wavelength photons and downshift them to longer wavelengths where the OPV device exhibits improved spectral response, thus generating enhanced photocurrent. Moreover, consistent trends with those found from the *J–V* characterization are also observed, with a maximum EQE exhibited for 1 wt% PB-dye concentration. As a result, the newly developed H-coating incorporating the luminescent PB-dye proved to be an effective LDS system for improved device performance in P3HT:PCBM-based OPVs.

It is worth noting that the previously discussed performance improvement observed upon application of our multifunctional LDS coating is in line with what theoretically expected from the downshifting process. In particular, as inferred from the

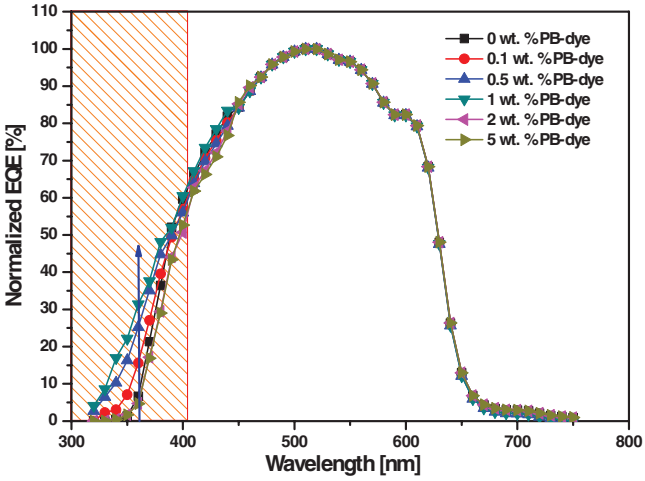

Figure 4. EQE curves for OPV devices coated with an LDS layer incorporating increasing concentrations of PB-dye.

standard reference solar spectra (ASTM G-173-03), the power density of UV photons (280–400 nm range) accounts for only a small fraction (about 9.3%) of the irradiance over the entire AM1.5G solar spectrum (≈1000 W m^{-2}).[21] Considering that the luminescent species incorporated in the LDS layer emits isotropically and that the critical angle for total internal reflection (TIR) in our system is about 43°, incident UV-photons absorbed and re-emitted by the PB-dye within the LDS layer at angles lower than this critical value are expected to leave the LDS layer through the escape cone. The probability of a photon to undergo TIR is given by the following expression[34]

$$P_{\mathrm{TIR}} = \sqrt{1 - \frac{n_{\mathrm{air}}^2}{n_{\mathrm{LDS}}^2}} \quad (1)$$

which is in our case of about 73% (n_{air} and n_{LDS} are the refractive indexes of air and of the LDS layer, respectively). In addition to this, a further 3%–4% incident photons are lost at the air/LDS layer interface for specular reflection. As a result, a maximum theoretical increase in performance of about 6.6% due to the downshifting of absorbed UV-photons can be expected upon the application of an LDS layer on the OPV devices. Based on these considerations, the maximum 4% PCE increase measured in this work in the presence of our new LDS coating clearly indicates the excellent operational capabilities of this new system (>60% of the maximum theoretically achievable PCE enhancement). To the best of our knowledge, this represents the highest PCE enhancement reported to date on flexible OPVs by means of a polymer-based LDS layer.

Considering the positive results obtained with LDS experiments in terms of OPV device performance improvement, a study on the long-term durability of devices was performed in order to investigate the possible beneficial effects of the luminescent layer on the performance evolution over prolonged light exposure time. Indeed, a stability enhancement could be expected due to the UV-screening functionality potentially provided by the luminophore incorporated into the LDS layer. To this end, a severe accelerated weathering test was conducted on different OPV device configurations for over 550 h in a weathering chamber with continuous intense light irradiation (1000 W m^{-2}), in the presence of 20% relative humidity and at constant temperature (38 °C). In addition to LDS-coated (1 wt% PB-dye) and control uncoated inverted flexible OPV devices, the performance evolution of flexible OPVs in standard configuration (PET-ITO/PEDOT:PSS/P3HT:PCBM/Ca/Al) encapsulated with commercial barrier foils was also evaluated as additional state-of-the-art reference device architecture. **Figure 5** illustrates the evolution of the normalized PCE over time for the considered device configurations during the entire duration of the weathering test. Clearly, the presence of an LDS layer is found to significantly improve the device stability compared to both uncoated and standard systems. In particular, LDS-coated devices were able to retain over 80% of their initial performance even after more than 550 h of continuous light exposure, while both uncoated and standard OPV systems were found to lose nearly 70% of their initial efficiency during the same testing time. The PCE decline over irradiation time observed on uncoated and standard OPVs is likely to be ascribed to the combined detrimental action on the OPV stack of UV-photons,

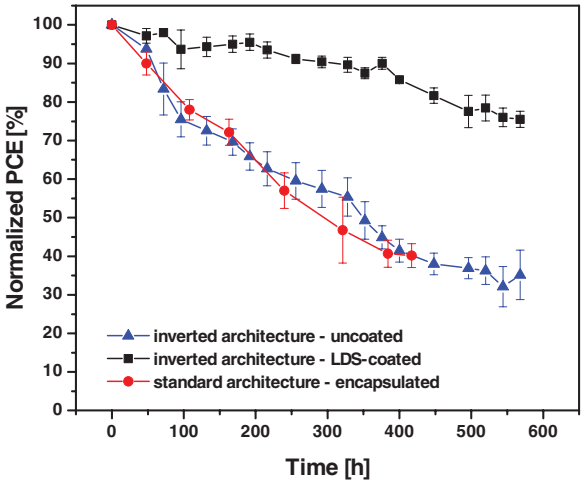

Figure 5. Normalized power conversion efficiency plot over light exposure time for uncoated reference devices, LDS-coated devices, and encapsulated devices in standard configuration.

oxygen, and moisture present in the testing environment. Indeed, it is well known that these factors can induce accelerated degradation pathways in OPVs (most notably, photooxidative degradation of the BHJ organic components, together with chemical and physical degradation of the buffer layers and electrode interfaces) that are typically responsible for the observed decline in device performance over time.[6,7,35] In addition, the relatively poor performance of OPV devices with standard architecture encapsulated with commercial barrier foils can be explained by considering the inferior stability of this device configuration, which is well-known to be highly prone to oxidation of the low work-function metal back electrode if compared to the inverted counterpart.[6,36] As opposed to this, the excellent stability of LDS-coated inverted devices can be directly correlated to the multifunctional nature of the new light-managing LDS layer proposed in this work. On one side, the presence of the PB-dye in the H-coating ensures an efficient UV screening action that prevents harmful incident UV photons to reach the underlying OPV device, thus significantly limiting its photodegradation. In this respect, the efficiency decay observed on uncoated devices with inverted architecture may be ascribed to different mechanisms acting simultaneously, namely photooxidation of the BHJ materials, together with chemical and physical degradation at the electrode interfaces and in the buffer layers, all negatively affecting the photovoltaic parameters.[6,7] More specifically, the reduction of V_{oc} and *FF* over time (Figure S6a,c in the Supporting Information) observed on uncoated OPV devices with inverted architecture may be correlated with changes in the energy levels of the donor polymer as well as UV-induced shunting in the ZnO layer.[37] In particular, this latter effect is further supported by the trends observed on devices with standard architecture (no ZnO layer in the stack sequence), for which V_{oc} is found to remain constant throughout the weathering test (Figure S6a in the Supporting Information). Additionally, the drop in *FF* and J_{sc} observed to different extents on both uncoated devices with inverted architecture and encapsulated OPVs with standard configuration may be ascribed to the degradation of the BHJ materials and the PEDOT:PSS hole transporting layer (Figure S6b,c in the Supporting Information).[6,7,38] In contrast to these behaviors, the presence of the LDS layer significantly reduces such UV-induced degradation pathways and imparts excellent stability to the LDS-coated systems. Furthermore, the fluorinated hybrid coating material provides a highly chemically stable environment for the luminescent chromophore, thus ensuring its prolonged durability over time even under aggressive irradiation conditions. In particular, compared to previously published work on polymeric LDS systems applied to dye-sensitized solar cells,[17] significantly improved photochemical stability during prolonged light exposure was observed with the newly designed sol–gel hybrid material presented in this work, thus demonstrating its excellent response even under harsh weathering conditions (see Supporting Information, Figure S7). Finally, the highly crosslinked hybrid nature of the H-coating (high T_g, low free-volume and low macromolecular chain mobility) may guarantee low gas (oxygen and moisture) permeability as a result of the limited free-volume available, further improving the barrier effect and lengthening OPV device lifetime.

It is worth mentioning that LDS-coated OPV devices were found to exhibit a similar performance behavior over irradiation time as that observed on analogous uncoated inverted OPVs encapsulated with commercial barrier foils (Supporting Information, Figure S4), further indicating the excellent stabilizing effect imparted by the new LDS hybrid coating material presented in this work.

3. Conclusion

In summary, a novel high-durability multifunctional organic–inorganic hybrid coating material was presented in this work for application as LDS host matrix system in flexible OPV devices. Such new LDS coating was obtained by incorporating a fluorescent organic dye in an appropriately functionalized fluoropolymeric resin that could be readily crosslinked in one-pot through a dual-cure ambient-temperature photo-induced sol–gel process. This system was employed as host matrix material for LDS layers on flexible OPV devices with inverted architecture, and a relative PCE improvement exceeding 4% was obtained compared to uncoated devices by carefully optimizing the concentration of the organic dye incorporated in the luminescent layer. To the best of our knowledge, this represents the highest PCE enhancement reported to date on flexible OPVs by means of a polymer-based LDS layer. In addition, long-term accelerated weathering tests (>550 h) highlighted the excellent stability of LDS-coated OPV devices that were able to retain 80% of their initial performance, as opposed to the dramatic efficiency drop experienced by control devices. Such remarkable behavior was attributed to the multifunctional nature of the newly proposed LDS-coating, which is able to provide simultaneous UV-screening action, intrinsic high chemical stability, and barrier effect, thus significantly lengthening OPV device lifetime.

The easily accessible one-step synthetic approach presented in this study to readily obtain a fully crosslinked hybrid film without the need of additional thermal post-treatments opens the way for the use of hybrid sol–gel systems onto heat-sensitive

substrates, thus paving the path for the straightforward fabrication of flexible devices with improved performance and enhanced stability without altering the chemistry of the photoactive layer.

4. Experimental Section

All reagents were purchased from Sigma-Aldrich and used as received, unless otherwise stated.

Device Preparation: OPV devices with inverted architecture were prepared using flexible PET/ITO substrates (R_s = 60 Ω sq^{-1}) rinsed with distilled water and acetone in an ultrasonic bath (10 min for each solvent). Then, they were treated with an oxygen plasma for 5 min. A buffer layer of zinc oxide was obtained via the sol–gel method.[39] The sol was prepared by mixing 200 mg of zinc acetate dihydrate (Alfa Aesar) with 55 µL of monoethanolamine (Alfa Aesar), 2 mL of 2-methoxyethanol, and 32.8 µL of water. Then, the sol was left under stirring overnight and filtered in a poly(tetrafluoroethylene) (PTFE) filter with 0.2 µm pore size prior to deposition by spin coating (1200 rpm, 40 s) on the ITO layer under ambient conditions. After deposition, substrates underwent a thermal annealing step at 140 °C for 1 h. Poly(3-hexylthiophene) (P3HT, Rieke Metals) and [6]-phenyl-C_{61}-butyric acid methyl ester (PCBM, Solenne) solutions in 1,2-dichlorobenzene with 40 mg mL^{-1} concentration were prepared in a nitrogen-filled glove box ([H_2O],[O_2] <0.5 ppm) and left under stirring on a hotplate at 50 °C overnight. At least 1 h prior to deposition, the stock solutions were mixed with weight ratio 1:1 to obtain the photoactive layer blend and left under stirring at 50 °C. Then, substrates were moved inside a nitrogen-filled glove box for the deposition of the photoactive layer by spin coating (700 rpm, 1 min). Substrates were placed under a Petri dish for solvent annealing, which lasted ≈1 h. Then, 2-propanol was spin cast on the substrates (two steps: 600 rpm, 5 s; 2000 rpm, 5 s) prior to screen printing the poly(3,4-ethylenedioxythiophene)-poly(styrenesulfonate) (PEDOT:PSS, Orgacon EL-P 5015, Agfa) buffer layer. Screen printing was performed in ambient conditions with a mask consisting of a mesh with 120 wires cm^{-1}. After printing, the substrates were moved inside the glove box for an annealing step at 110 °C for 10 min. To complete the cell stack sequence, a silver paste (Solamet PV410, DuPont) was screen printed on top of the PEDOT:PSS in ambient conditions. Then, substrates were moved inside a nitrogen-filled glove box for a thermal annealing step carried out at 140 °C for 15 min. Fabricated devices were encapsulated with PET foils (Hostaphan GN 4600, Mitsubishi Polyester Films) and a pressure sensitive adhesive (467 MP, 3 M), which were cold-laminated using a Yosan LM-260 laminator machine. Copper tape lined with an acrylic conductive adhesive (Advanced Tapes) and press fasteners (Prym Jersey) were used for external contact of the sealed devices.

OPV devices with standard architecture were prepared using commercial ITO-PET substrate (CP Films 50 Ω sq^{-1}). The sputtered ITO-PET was patterned in a rotary screen printing process using an etching paste (Merck, Isishape Hiperetch). Hole transporting layer of PEDOT:PSS (Clevios P VP AI4083: 2-propanol with the ratio of 75:25 wt%) and photoactive layer of P3HT:PCBM (Rieke metals and Nano-C: 131 mg mL^{-1} in 1.2-dichlorobenzene) were processed with sheet based gravure printing machine (Schläfli Labratester) with a line density of 100 lines cm^{-1} and 120 lines cm^{-1}. After printing, the substrates were transferred into the glove box and annealed on a hot plate at 120 °C for 10 min prior to the thermal evaporation of Ca/Ag. Process details of OPV devices are described in detail in the paper by Apilo et al.[40] Finally, OPV devices were encapsulated with a commercial gas barrier foil (3M FTB3-125) using cold lamination process (Yosan LM-260).

Testing of the photovoltaic devices was performed under 1 sun AM1.5G illumination, provided by a Sun 2000 solar simulator (ABET Technologies) and by using a Keithley 2612B source measuring unit to carry out the potential scans. Multiple tests were performed on the devices, as their PV response improved upon exposure to the simulated solar light, until a maximum value was attained. This testing methodology is common practice in the field of OPVs and is typically originated from reversible adsorption of oxygen on the ZnO electron transport layer, which is desorbed upon exposure to the UV portion of solar light (the so-called light soaking process).[41]

Data presented for each condition were averaged on at least three OPV devices. EQE measurements were performed in direct-current (DC) mode using a 100 W QTH lamp (Newport) as light source and a 150 mm Czerny Turner monochromator (Omni-λ 150, Lot-Oriel, Darmstadt, Germany).

OPV devices were subjected to weathering tests under continuous Xenon light illumination in a weather-o-meter chamber (Solarbox 3000e, Cofomegra S.r.l.) equipped with an outdoor filter cutting all wavelengths below 280 nm. The weathering test was conducted in compliance with the ISOS-L-1 standard.[42] The total irradiance was measured by means of a power-meter with thermopile sensor (Ophir) and found to be ≈1000 W m^{-2} (550 W m^{-2} in the 300–800 nm wavelength range) for the entire duration of the test (>550 h). The UV-light irradiance level in the 295–400 nm range was 50 W m^{-2}, as measured by means of a UV-photodiode. The relative humidity and the working temperature inside the test chamber were maintained constant and measured to be 20% and 38 °C, respectively. The black standard temperature was 65 °C for the entire duration of the test.

Synthesis of the UV- and Thermo-Curable Fluorinated Resin: Lumiflon LF-910LM (AGC Chemicals Americas), a commercially available CTFE-VE copolymer, was functionalized with 2-isocyanatoethyl methacrylate (IEM, Showa Denko) and 3-(triethoxysilyl)propyl isocyanate (IPTES). To obtain a photo-induced sol–gel transition on the crosslinkable resin, all the —OH groups in the CTFE-VE copolymer were functionalized with IEM and IPTES (eqOH:eqNCO_{IEM}:eqNCO_{IPTES} = 1:0.5:0.5), leading to the formation of urethane bonds (Scheme 1).

The typical functionalization process consisted in mixing 40 g of Lumiflon with 3.7 g of IEM and 5.9 g of IPTES in a three-neck round-bottom flask equipped with a condenser. The reaction was catalyzed by di-*n*-butyltin dilaurate (DBTDL) at a 0.3 wt% concentration with respect to the dry polymer. The catalyst was added to the reaction mixture as a 1 wt% solution in ethyl acetate (7.9 g of solution containing 79 mg of DBTDL). The reaction was carried out in an inert atmosphere (nitrogen) at 75 °C under continuous stirring. During reaction, the flask was covered with an aluminum foil to keep the mixture under dark conditions.

The extent of the reaction was monitored by measuring FTIR spectra of the resin at increasing reaction times. The disappearance of the isocyanate (NCO) peak at 2270 cm^{-1} was controlled as an indication of the complete occurrence of the functionalization reaction. After 3 h, the NCO peak completely disappeared and the process was terminated.

The final product (MS-resin) was diluted in EtOH at 50 wt% and stored in the dark.

Synthesis of the Fluorescent Organic Dye Trans-5-(p-(N,N-diphenylamino)styril)-1,3-di(2-pyridyl)-benzene (PB-Dye): A mixture of 1,3-dibromobenzyl bromide (1.81 g, 5.49 mmol) and triethyl phosphite (4.5 ml, 26.2 mmol) was heated and stirred under argon at 160 °C for 6 h to give the diethylphosphonate ester. The excess of triethyl phosphite and byproducts was then removed by heating at 100 °C under vacuum for several hours. After that, potassium tert-butoxide (1.93 g, 17.08 mmol) was slowly added to a solution of 1,3-dibromo-5-diethoxy-phosphorylmethylbenzene (1.79 g, 4.64 mmol) and 4-(diphenylamino)benzaldehyde (1.79 g, 6.57 mmol) in dry tetrahydrofuran (THF, 50 mL) cooled to 0 °C under a nitrogen atmosphere. The cool bath was then removed and the mixture was stirred at room temperature overnight. After hydrolysis with water, the mixture was stirred for a further 30 min, diluted with ethyl acetate (AcOEt) and washed with water. The organic layer was dried over anhydrous Na_2SO_4 and concentrated. The pure trans-5-(p-(N,N-diphenylamino)styryl)-1,3-dibromo benzene was obtained as a pale yellow solid (1.98 g, 84%) by flash chromatography using hexane/acetate 9:1 as eluant. Under an argon atmosphere, a mixture of the 5-substituted 1,3-dibromobenzene derivative (1.98 g, 3.92 mmol),

2-(tri-n-butylstannyl)pyridine (4.53 g, 11.76 mmol), $PdCl_2(PPh_3)_2$ (83 mg, 0.12 mmol), LiCl (1.48 g, 35.28 mmol), and dry toluene (24 mL) was stirred at 111 °C for 24 h. After cooling to room temperature, 50 mL of NaOH (1 M in water) were added to the reaction mixture and the product was extracted with ethylacetate. The organic layer was washed with water and dried over anhydrous Na_2SO_4 and the solvent was removed under reduced pressure. The pure compound was obtained by flash chromatography on silica gel eluting with hexane/ethyl acetate 8:2 (800 mg, 41%). Nuclear magnetic resonance (NMR) spectra are in agreement with those previously reported.[29]

Luminescent Sol–Gel Coating Formulation and Deposition: Starting from the diluted MS-resin, a hybrid sol–gel formulation was prepared containing silica as inorganic component. The silica precursor used here was TEOS. The molar ratios between the components in the starting sol were TEOS:EtOH:H_2O:HCl = 1:4.5:3.5:0.07 and the theoretical composition of the resulting gel is given in Table S1 (Supporting Information). The sol consisted of a mixture of MS-resin and TEOS, diluted in EtOH. After 1 h of magnetic stirring, an aqueous solution of hydrochloric acid (HCl, 3.4 wt%) was added dropwise to the sol. An additional hour of stirring ensured the complete occurrence of TEOS hydrolysis. Then, the sol was left at rest for 24 h before deposition, to avoid opacity in the resulting film. Irgacure TPO-L (BASF) was added as radical photoinitiator, at 3 wt% concentration with respect to the dry polymer. PB-dye was employed as luminescent species in different concentrations (0.1-0.5-1-2-5 wt% with respect to the dry polymer). Solutions containing the luminescent species were usually prepared at least one hour before deposition and left under stirring. Irgacure TPO-L was added to the reactive mixture in the dark inside the glove-box just before deposition of the coating to avoid undesired crosslinking reactions triggered by visible light upon stirring.

Deposition of the coatings was performed in a glove box by spin coating (1200 rpm, 40 s). UV-curing was carried out with two portable low-power UV torches (3W 405 nm UV LED, UltraFire WF-501B) under nitrogen atmosphere for 150 s.

Materials Characterization: FTIR spectroscopy was performed in transmission mode in air at room temperature with a FT/IR-615 spectrophotometer (Jasco Inc.) to evaluate the progress of the functionalization reactions. FTIR spectra were taken using NaCl round crystal disks. UV–visible spectroscopy analyses were performed in air at room temperature with an Evolution 600 UV–vis spectrophotometer (Thermo Scientific). Fluorescence spectra were measured in air at room temperature by using a Jasco FP-6600 Spectrofluorometer. The excitation wavelength was 350 nm. Evaluation of solvent resistance was performed by solvent rub test, according to the standard ASTM D4752.[25] DSC analyses were performed by means of a DSC 823e (Mettler-Toledo) instrument. The measurements consisted of three heating/cooling runs: from 25 to 200 °C at 20 °C min^{-1}, from 200 to 0 °C at 20 °C min^{-1}, and from 0 to 200 °C at 20 °C min^{-1}. TGA was performed both under air and nitrogen flux with a TGA Q 500 (TG Instruments). Static optical contact angle measurements on the LDS hybrid coating were performed with an OCA 20 (DataPhysics) equipped with a CCD photo-camera and with a 500 µL Hamilton syringe to dispense liquid droplets. Measurements were taken at room temperature via the sessile drop technique. At least 20 measurements were performed in different regions on the surface of each coating and results were averaged. Water and diiodomethane were used as probe liquids. Coating depositions were performed with a WS-650MZ-23NPP (Laurell) spin coater, which was located inside a nitrogen-filled glove box. Optical microscopy was performed by using an Olympus BX-60 reflected-light optical microscope equipped with an Infinity 2 digital camera and able to operate both in bright-field and dark-field.

Supporting Information

Supporting Information is available from the Wiley Online Library or from the author.

Acknowledgements

C.D. thanks Università degli Studi di Milano for financial support (Piano Sostegno alla Ricerca 2015–17 -LINEA 2 Azione A – Giovani Ricercatori).

Received: July 21, 2016
Published online: October 10, 2016

[1] a) H. Spanggaard, F. C. Krebs, *Sol. Energy Mater. Sol. Cells* **2004**, *83*, 125; b) G. Li, R. Zhu, Y. Yang, *Nat. Photon.* **2012**, *6*, 153.

[2] C. C. Chen, W. H. Chang, K. Yoshimura, K. Ohya, J. You, J. Gao, Z. Hong, Y. Yang, *Adv. Mater.* **2014**, *26*, 5670.

[3] L. Dou, J. You, J. Yang, C.-C. Chen, Y. He, S. Murase, T. Moriarty, K. Emery, G. Li, Y. Yang, *Nat. Photon.* **2012**, *6*, 180.

[4] a) N. Blouin, A. Michaud, M. Leclerc, *Adv. Mater.* **2007**, *19*, 2295; b) P. L. T. Boudreault, A. Najari, M. Leclerc, *Chem. Mater.* **2011**, *23*, 456; c) H. Y. Chen, J. Hou, S. Zhang, Y. Liang, G. Yang, Y. Yang, L. Yu, Y. Wu, G. Li, *Nat. Photon.* **2009**, *3*, 649; d) T. Y. Chu, J. Lu, S. Beaupré, Y. Zhang, J. R. Pouliot, S. Wakim, J. Zhou, M. Leclerc, Z. Li, J. Ding, Y. Tao, *J. Am. Chem. Soc.* **2011**, *133*, 4250; e) J. Hou, H. Y. Chen, S. Zhang, R. I. Chen, Y. Yang, Y. Wu, G. Li, *J. Am. Chem. Soc.* **2009**, *131*, 15586; f) R. Kroon, M. Lenes, J. C. Hummelen, P. W. M. Blom, B. De Boer, *Polym. Rev.* **2008**, *48*, 531; g) Y. Li, Y. Zou, *Adv. Mater.* **2008**, *20*, 2952; h) Y. Liang, Y. Wu, D. Feng, S. T. Tsai, H. J. Son, G. Li, L. Yu, *J. Am. Chem. Soc.* **2009**, *131*, 56; i) C. Winder, N. S. Sariciftci, *J. Mater. Chem.* **2004**, *14*, 1077.

[5] a) J. Y. Kim, K. Lee, N. E. Coates, D. Moses, T. Q. Nguyen, M. Dante, A. J. Heeger, *Science* **2007**, *317*, 222; b) W. Li, A. Furlan, K. H. Hendriks, M. M. Wienk, R. A. J. Janssen, *J. Am. Chem. Soc.* **2013**, *135*, 5529; c) S. Sista, M. H. Park, Z. Hong, Y. Wu, J. Hou, W. L. Kwan, G. Li, Y. Yang, *Adv. Mater.* **2010**, *22*, 380; d) J. You, C. C. Chen, Z. Hong, K. Yoshimura, K. Ohya, R. Xu, S. Ye, J. Gao, G. Li, Y. Yang, *Adv. Mater.* **2013**, *25*, 3973; e) J. You, L. Dou, K. Yoshimura, T. Kato, K. Ohya, T. Moriarty, K. Emery, C. C. Chen, J. Gao, G. Li, Y. Yang, *Nat. Commun.* **2013**, *4*, 1446.

[6] M. Jørgensen, K. Norrman, S. A. Gevorgyan, T. Tromholt, B. Andreasen, F. C. Krebs, *Adv. Mater.* **2012**, *24*, 580.

[7] M. Jørgensen, K. Norrman, F. C. Krebs, *Sol. Energy Mater. Sol. Cells* **2008**, *92*, 686.

[8] a) M. S. Abdou, S. Holdcroft, *Macromolecules* **1993**, *26*, 2954; b) M. Manceau, A. Rivaton, J.-L. Gardette, S. Guillerez, N. Lemaître, *Polym. Degrad. Stab.* **2009**, *94*, 898; c) A. Aguirre, S. Meskers, R. Janssen, H.-J. Egelhaaf, *Org. Electron.* **2011**, *12*, 1657; d) G. Griffini, S. Turri, M. Levi, *Polym. Bull.* **2011**, *66*, 211.

[9] a) M. Drees, H. Hoppe, C. Winder, H. Neugebauer, N. S. Sariciftci, W. Schwinger, F. Schäffler, C. Topf, M. C. Scharber, Z. Zhu, *J. Mater. Chem.* **2005**, *15*, 5158; b) B. J. Kim, Y. Miyamoto, B. Ma, J. M. Frechet, *Adv. Funct. Mater.* **2009**, *19*, 2273; c) M. S. Ryu, J. Jang, *Sol. Energy Mater. Sol. Cells* **2010**, *94*, 1384; d) D. Sahu, H. Padhy, D. Patra, D. Kekuda, C.-W. Chu, I.-H. Chiang, H.-C. Lin, *Polymer* **2010**, *51*, 6182; e) J. Farinhas, Q. Ferreira, R. E. Di Paolo, L. Alcácer, J. Morgado, A. Charas, *J. Mater. Chem.* **2011**, *21*, 12511; f) G. Griffini, J. D. Douglas, C. Piliego, T. W. Holcombe, S. Turri, J. M. Fréchet, J. L. Mynar, *Adv. Mater.* **2011**, *23*, 1660.

[10] a) F. C. Krebs, H. Spanggaard, *Chem. Mater.* **2005**, *17*, 5235; b) M. H. Petersen, S. A. Gevorgyan, F. C. Krebs, *Macromolecules* **2008**, *41*, 8986; c) M. Helgesen, S. A. Gevorgyan, F. C. Krebs, R. A. Janssen, *Chem. Mater.* **2009**, *21*, 4669; d) M. Helgesen, F. C. Krebs, *Macromolecules* **2010**, *43*, 1253; e) F. C. Krebs, K. Norrman, *ACS Appl. Mater. Interfaces* **2010**, *2*, 877.

[11] a) G. Dennler, C. Lungenschmied, H. Neugebauer, N. Sariciftci, A. Labouret, *J. Mater. Res.* **2005**, *20*, 3224; b) P. Madakasira, K. Inoue, R. Ulbricht, S. B. Lee, M. Zhou, J. P. Ferraris,

A. A. Zakhidov, *Synth. Met.* **2005**, *155*, 332; c) G. Dennler, C. Lungenschmied, H. Neugebauer, N. Sariciftci, M. Latreche, G. Czeremuszkin, M. Wertheimer, *Thin Solid Films* **2006**, *511*, 349; d) A. J. Medford, M. R. Lilliedal, M. Jørgensen, D. Aarø, H. Pakalski, J. Fyenbo, F. C. Krebs, *Opt. Express* **2010**, *18*, A272; e) F. C. Krebs, J. Fyenbo, D. M. Tanenbaum, S. A. Gevorgyan, R. Andriessen, B. van Remoortere, Y. Galagan, M. Jørgensen, *Energy Environ. Sci.* **2011**, *4*, 4116.

[12] M. Kennedy, H. Ahmed, J. Doran, B. Norton, P. Bosch-Jimenez, M. Della Pirriera, E. Torralba-Calleja, D. Gutiérrez Tauste, L. Aubouy, S. Daren, F. Solomon-Tsvetkov, S. Galindo, C. Voz, J. Puigdollers, *Phys. Status Solidi A* **2015**, *212*, 203.

[13] H. Hovel, R. Hodgson, J. Woodall, *Sol. Energy Mater.* **1979**, *2*, 19.

[14] E. Klampaftis, D. Ross, K. R. McIntosh, B. S. Richards, *Sol. Energy Mater. Sol. Cells* **2009**, *93*, 1182.

[15] D. Alonso-Álvarez, D. Ross, E. Klampaftis, K. R. McIntosh, S. Jia, P. Storiz, T. Stolz, B. S. Richards, *Prog. Photovolt. Res. Appl.* **2015**, *23*, 479.

[16] F. Bella, G. Griffini, M. Gerosa, S. Turri, R. Bongiovanni, *J. Power Sources* **2015**, *283*, 195.

[17] G. Griffini, F. Bella, F. Nisic, C. Dragonetti, D. Roberto, M. Levi, R. Bongiovanni, S. Turri, *Adv. Energy Mater.* **2015**, *5*, 1401312.

[18] a) L. Slooff, R. Kinderman, A. Burgers, N. Bakker, J. Van Roosmalen, A. Büchtemann, R. Danz, M. Schleusener, *J. Sol. Energy Eng.* **2007**, *129*, 272; b) S. Engmann, M. Machalett, V. Turkovic, R. Rösch, E. Rädlein, G. Gobsch, H. Hoppe, *J. Appl. Phys.* **2012**, *112*, 034517; c) M. Prosa, A. Sagnella, T. Posati, M. Tessarolo, M. Bolognesi, S. Cavallini, S. Toffanin, V. Benfenati, M. Seri, G. Ruani, M. Muccini, R. Zamboni, *RSC Adv.* **2014**, *4*, 44815; d) M. Dusza, M. Stefanski, M. Wozniak, D. Hreniak, Y. Gerasymchuk, L. Marciniak, F. Granek, W. Strek, *J. Lumin.* **2016**, *169*, 857; e) A. J. Das, K. Narayan, *Adv. Mater.* **2013**, *25*, 2193; f) O. Moudam, N. Bristow, S.-W. Chang, M. Horie, J. Kettle, *RSC Adv.* **2015**, *5*, 12397.

[19] M. Nam, H. K. Kwon, S. J. Kwon, S. H. Kwon, M. Cha, S. H. Lee, S. Park, D. Jeong, K. T. Lee, H. Rhee, *Adv. Energy Mater.* **2016**, *6*, 1500424.

[20] G.-F. Ma, H.-J. Xie, P.-P. Cheng, Y.-Q. Li, J.-X. Tang, *Appl. Phys. Lett.* **2013**, *103*, 043302.

[21] J. Kettle, N. Bristow, D. Gethin, Z. Tehrani, O. Moudam, B. Li, E. Katz, G. A. dos Reis Benatto, F. C. Krebs, *Sol. Energy Mater. Sol. Cells* **2016**, *144*, 481.

[22] a) B. G. Ranby, J. F. Rabek, *Photodegradation, Photo-oxidation, and photostabilization of polymers*, Wiley, New York **1975**; b) H. Kaczmarek, A. Kamińska, A. van Herk, *Eur. Polym. J.* **2000**, *36*, 767.

[23] U. Schubert, N. Hüsing, A. Lorenz, *Chem. Mater.* **1995**, *7*, 2010.

[24] a) L. L. Hench, in *Science of Ceramic Processing*, Wiley-Interscience, New York **1986**, p. 52; b) L. L. Hench, G. Orcel, *J. Non-Cryst. Solids* **1986**, *82*, 1 ; c) W. Klemperer, V. Mainz, S. Ramamurthi, F. Rosenberg, C. Brinker, D. Clark, D. Ulrich, *Mater. Res. Soc.* **1988**, *121*, 15; d) G. Orcel, L. L. Hench, I. Artaki, J. Jonas, T. Zerda, *J. Non-Cryst. Solids* **1988**, *105*, 223; e) C. Brinker, G. Scherer, *Sol-Gel Science*, Academic Press, San Diego, CA **1990**.

[25] Practice for Measuring MEK Resistance of Ethyl Silicate (Inorganic) Zinc-Rich Primers by Solvent Rub, ASTM D4752.

[26] a) A. Al-Sabounchi, *Renew. Energ.* **1998**, *14*, 149; b) M. A. García, J. Balenzategui, *Renew. Energ.* **2004**, *29*, 1997.

[27] a) D. K. Owens, R. Wendt, *J. Appl. Polym. Sci.* **1969**, *13*, 1741; b) D. Kaelble, *J. Adhesion* **1970**, *2*, 66; c) W. Rabel, *Farbe und Lack* **1971**, *77*, 997.

[28] M. T. Dang, L. Hirsch, G. Wantz, *Adv. Mater.* **2011**, *23*, 3597.

[29] a) F. Nisic, A. Colombo, C. Dragonetti, D. Roberto, A. Valore, J. M. Malicka, M. Cocchi, G. R. Freeman, J. A. G. Williams, *J. Mater. Chem. C* **2014**, *2*, 1791; b) F. Nisic, A. Colombo, C. Dragonetti, M. Fontani, D. Marinotto, S. Righetto, D. Roberto, J. A. G. Williams, *J. Mater. Chem. C* **2015**, *3*, 7421.

[30] D. Alonso-Álvarez, D. Ross, B. S. Richards, presented at *Photovoltaic Specialists Conf. (PVSC), 2012 38th IEEE*, 3-8 June **2012**, Austin, Texas.

[31] G. Griffini, M. Levi, S. Turri, *Renew. Energ.* **2015**, *78*, 288.

[32] a) C. Haines, M. Chen, K. P. Ghiggino, *Sol. Energy Mater. Sol. Cells* **2012**, *105*, 287; b) H. Yoo, J. Yang, A. Yousef, M. R. Wasielewski, D. Kim, *J. Am. Chem. Soc.* **2010**, *132*, 3939.

[33] L. E. Noreña-Franco, F. Kvasnik, *Analyst* **1998**, *123*, 2185.

[34] M. J. Currie, J. K. Mapel, T. D. Heidel, S. Goffri, M. A. Baldo, *Science* **2008**, *321*, 226.

[35] a) W. Cai, X. Gong, Y. Cao, *Sol. Energy Mater. Sol. Cells* **2010**, *94*, 114; b) C. J. Brabec, S. Gowrisanker, J. J. M. Halls, D. Laird, S. Jia, S. P. Williams, *Adv. Mater.* **2010**, *22*, 3839.

[36] B. P. Rand, H. Richter, *Organic Solar Cells: Fundamentals, Devices, and Upscaling*, CRC Press, Boca Raton, FL **2014**.

[37] a) A. Manor, E. A. Katz, T. Tromholt, F. C. Krebs, *Adv. Energy Mater.* **2011**, *1*, 836; b) H. Hintz, H. J. Egelhaaf, H. Peisert, T. Chassé, *Polym. Degrad. Stab.* **2010**, *95*, 818.

[38] K. Norrman, M. V. Madsen, S. A. Gevorgyan, F. C. Krebs, *J. Am. Chem. Soc.* **2010**, *132*, 16883.

[39] G. Iannaccone, A. Bernardi, R. Suriano, C. L. Bianchi, M. Levi, S. Turri, G. Griffini, *RSC Adv.* **2016**, *6*, 46915.

[40] P. Apilo, J. Hiltunen, M. Välimäki, S. Heinilehto, R. Sliz, J. Hast, *Prog. Photovolt: Res. Appl.* **2014**, *23*, 918.

[41] M. R. Lilliedal, A. J. Medford, M. V. Madsen, K. Norrman, F. C. Krebs, *Sol. Energy Mater. Sol. Cells* **2010**, *94*, 2018.

[42] M. O. Reese, S. A. Gevorgyan, M. Jørgensen, E. Bundgaard, S. R. Kurtz, D. S. Ginley, D. C. Olson, M. T. Lloyd, P. Morvillo, E. A. Katz, A. Elschner, O. Haillant, T. R. Currier, V. Shrotriya, M. Hermenau, M. Riede, K. R. Kirov, G. Trimmel, T. Rath, O. Inganäs, F. Zhang, M. Andersson, K. Tvingstedt, M. Lira-Cantu, D. Laird, C. McGuiness, S. Gowrisanker, M. Pannone, M. Xiao, J. Hauch, R. Steim, D. M. DeLongchamp, R. Rösch, H. Hoppe, N. Espinosa, A. Urbina, G. Yaman-Uzunoglu, J.-B. Bonekamp, A. J. J. M. van Breemen, C. Girotto, E. Voroshazi, F. C. Krebs, *Sol. Energy Mater. Sol. Cells* **2011**, *95*, 1253.